Particle
& Particle Systems Characterization
www.particle-journal.com

Particle-Arrayed Silver Mesocubes Synthesized via Reducing Silver Oxide Mesocrystals for Surface-Enhanced Raman Spectroscopy

Zhongbo Yang, Lei Zhang, Hongjun You, Zhiyuan Li, and Jixiang Fang**

In this study, we demonstrate an easy particle-mediated protocol using the specific structure of mesocrystal Ag_2O sacrificial templates to synthesize highly rough-cubic Ag mesocages. To the best of our knowledge, the mesocrystal particles are reported for the first time as sacrificial templates for synthesizing metal particles. The obtained Ag mesocages show high surface-enhanced Raman scattering (SERS) sensitivity because of the highly rough topography formed by arrays of uniform individual Ag nanoparticles. Abundant "hot spots" with greatly enhanced local electromagnetic field are promoted densely on the mesocage surface by the plenty of deep and narrow gaps and the hollow structure. The single-particle SERS signal generated by the Ag mesocage has an enhancement factor of approximately 10^9, which is approximately four times higher than the Ag mesocage synthesized using single-crystal Ag_2O particle as a template. Meanwhile, this signal displays a linear dependence on the detected analyte concentration, sensitively down to 1.0×10^{-12} M.

1. Introduction

Hollow nanostructures made of metals are intriguing to synthesize and study because they exhibit surface plasmonic properties and catalytic activities different from their solid counterparts.[1–3] When used as an optical device, the hollow structure offers great advantages in tuning the surface plasmon resonance.[1] Strong plasmonic field is produced from the coupling between the external and internal surface plasmon field in the hollow particles.[4] Thus, greatly enhanced Raman scattering can be obtained owing to the strong localized electric filed excited on the nanostructed shells.[5] Surface-enhanced Raman scattering (SERS)-based signal detection and molecular identification are new, powerful spectroscopy techniques attracting considerable interests in the fields of nanomaterials, biotechnologies, chemical analysis, and environmental monitoring.[6–13] At present, the fabrication of SERS substrates with a stable, uniform, and high average enhancement factor over relatively large areas remains a great challenge.[7,14–18] With the aim of creating a high amount of effective "hot spots" within individual particle, and simultaneously keeping high reliability and reproducibility, various metal particles with highly rough surfaces have been fabricated. Single-particle SERS enhancement factors of these particles are in the order of 10^5 to 10^6 for Ag star-like particles,[19] 10^6 to 10^7 for Au meatball-like and flower-like particles,[14,20,21] and 10^7 to 10^8 for Au urchin-like and Ag flower-like particles.[14,15,22] Recently, some hollow or porous metal nanostructured substrates show even higher enhancement (enhancement factors reach to 10^9).[23,24]

Up to now, many synthesis methods have been developed to prepare hollow metal particles.[25,26] The most commonly used method is the sacrificial template-directed protocol developed by Xia et al.[2,3,27] Metal nanocages can be prepared using various nanoparticles, such as silver,[28,29] nickel,[30] cobalt,[31] cuprous oxide,[32,33] silver oxide,[23] etc., with a range of morphologies as a sacrificial template by galvanic or reduction reaction. However, only single-crystal nanoparticles are mainly used as a sacrificial template that results in a relatively monotonous structure and surface topography. No study has yet reported on the use of mesocrystal particles as a sacrificial template to prepare hollow or porous particles. Mesocrystals are a newly found crystal structure that consist of an ordered mesoscale superstructure composed of individual nanocrystals aligned along a common crystallographic direction; they exhibit scattering properties similar to those of a single crystal.[25,34,35] Mesocrystal Ag_2O polyhedral particles can be prepared in situ through an external electric field-driven particle-mediated "bottom-up" assembling methodology.[36]

In this study, we found that mesocrystal Ag_2O polyhedral particles are more robust as sacrificial templates for the synthesis of Ag particles with controllable surface roughness and inner structure compared with single-crystal Ag_2O particles. In the reduction of the mesocrystal Ag_2O particle used as a sacrificial template, which is different from reduction using single-crystal Ag_2O particles, every nanocrystal unit in the mesocrystal can be separately reduced into small individual Ag nanoparticles with various structures depending on the reduction conditions. The produced small nanstructured Ag particles can self-assemble to

Z. B. Yang, L. Zhang, Dr. H. J. You, Prof. J. X. Fang
School of Science
Xi'an Jiaotong University
Shannxi 710049, P. R. China
E-mail: hjyou@mail.xjtu.edu.cn; jxfang@mail.xjtu.edu.cn
Prof. Z. Y. Li
Institute of Physics, Chinese Academy of Sciences
Beijing 100090, P. R. China

DOI: 10.1002/ppsc.201300290

form hollow or porous mesoparticles with controllable surface topography, which can serve as an ideal target for systematically investigating the influence of particle surface topography and inner structure on the SERS properties. It offers a new perspective because rough surfaces and hollow/porous structures have only been separately studied in the past.[23,24] Using mesocrystal Ag_2O polyhedrons as a sacrificial template, highly rough Ag mesocages can be obtained that show higher enhancement (approximately four times higher) for SERS than Ag mesocages synthesized using single-crystal Ag_2O particles as a sacrificial template.[23] Compared with Au particles with 1 nm nanobridged nanogaps,[16] each highly rough Ag mesocage has more nanogaps. Additionally, compared with urchin-like, meatball-like, and flower-like particles,[14,15,20,37] the hollow structure of this Ag mesocage can promote the enhancement of a local electromagnetic field on the surface,[4] thereby resulting in an amplified SERS signal. The synthetic principle and strategies reported herein using mesocrystal particles as templates open avenues for fabricating superstructures using specific mesocrystal structures to obtain higher SERS or other functional properties.

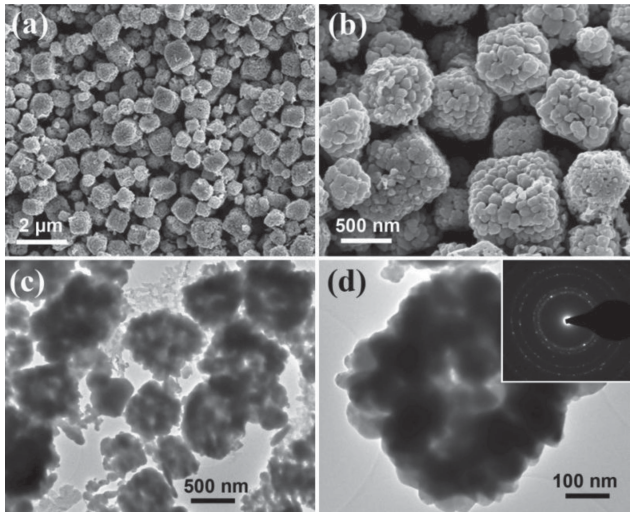

Figure 2. a,b) SEM and c,d) TEM images of highly rough Ag mesocages synthesized using mesocrystal Ag_2O cubes as sacrificial templates under fast reduction (10% H_2O_2, 120 s). The inset in d shows the correlated SAED patterns of a single Ag mesocage.

2. Results and Discussion

2.1. Morphology Control of Silver Mesoparticles

The protocol we used to synthesize silver mesoparticles with controllable roughness is based on the reduction of mesocrystal Ag_2O particles using hydrogen peroxide. In our previous study, single-crystal Ag_2O particles have been used as sacrificial templates to synthesize silver mesocages.[23] In the present study, mesocrystal Ag_2O particles were used to replace single-crystal Ag_2O particles as sacrificial templates for synthesizing silver mesocages. Mesocrystal cubic Ag_2O template particles were first synthesized using an electrochemical method.[36] **Figure 1** shows the scanning electron microscopy (SEM) images of the mesocrystal Ag_2O particles. The side lengths of the mesocrystal Ag_2O cubes are approximately 800 nm. By comparison, single-crystal Ag_2O particles with similar shapes and sizes were also synthesized by reactions among $AgNO_3$, ammonia, and NaOH, with PVP as surfactant ligand (SEM images in Figure S1, Supporting Information).[23] The crystal structures of mesocrystal and single-crystal Ag_2O template particles have been clearly presented in our previous reports.[23,36]

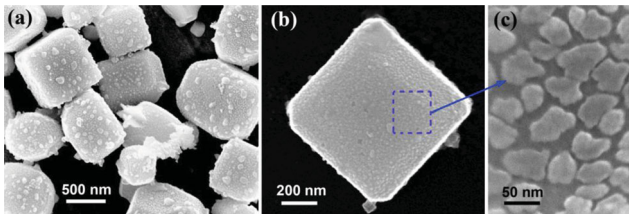

Figure 1. a) SEM image of cubic mesocrystal silver (I) oxide (Ag_2O) particles. b,c) SEM images of a single-mesocrystal Ag_2O particle and its surface morphology.

The mesocrystal Ag_2O particles demonstrate a growth mechanism different from the single-crystal Ag_2O particles. The single-crystal Ag_2O particles are formed through a classical atom/ion-mediated growth model. In the growth process, the primary growth units are atoms/ions that build onto the particle through diffusion and result in the single-crystal structure and smooth surface, as shown in Figure S1b (Supporting Information). While, the mesocrystal Ag_2O particles are formed through a non-classical particle-mediated growth model.[25,35] In the electrodeposition process, the increased Ag atoms in the solution aggregate to form small nanoparticles that are oxidized by dissolved oxygen in the solution to form Ag_2O nanoparticles. The small Ag_2O nanoparticles act as building units to assemble the mesocrystal Ag_2O particles through an oriented attachment mechanism.[38] In this particle-mediated growth, the primary growth units are small Ag_2O nanoparticles that still can be clearly seen on the particle-aggregated rough surface of mesocrystal Ag_2O particles (Figure 1b,c).

Compared with single-crystal Ag_2O particle templates, different Ag particles can be obtained using mesocrystal Ag_2O particles as sacrificial templates. **Figure 2** shows the SEM and transmission electron microscopy (TEM) images of highly rough Ag mesocages synthesized using the mesocrystal Ag_2O particles as sacrificial templates through quick reduction with H_2O_2 (10% H_2O_2, 120 s). The Ag mesocages inherit the shape and size of the mesocrystal Ag_2O particle templates well and show a highly rough surface (Figure 2a). The magnified SEM image in Figure 2b shows that the rough surface is composed of numerous uniform individual spherical nanoparticles. The TEM image in Figure 2c clearly displays the hollow interior. The strong contrast difference between the edges (dark) and center (bright) in the TEM image implies that the mesocages have a wall thickness of approximately 200–300 nm. The magnified TEM image in

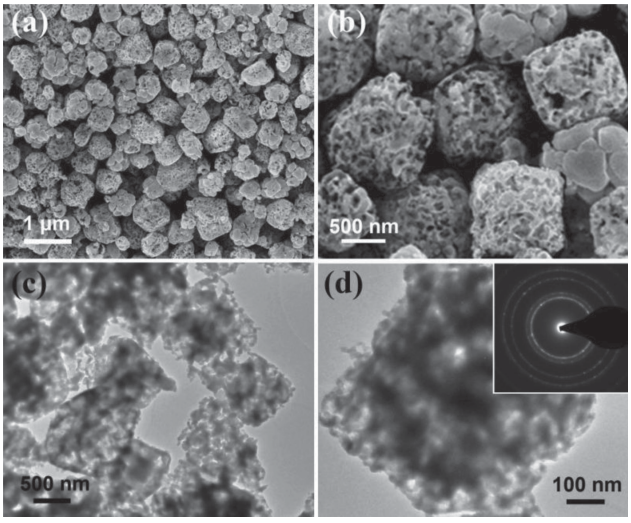

Figure 3. a,b) SEM and c,d) TEM images of porous Ag mesocubes synthesized using mesocrystal Ag_2O particles as sacrificial templates under slow reduction (1% H_2O_2, 120 s). The inset in (d) is the correlated SAED patterns of a single Ag mesocage.

Figure 2d shows that the wall of the mesocage is composed of nanoparticles. Selected-area electron diffraction (SAED) patterns (inset in Figure 2d) recorded from a single mesocage reveal the typical polycrystalline nature of all cubic Ag mesocages.

The surface topography and inner structure of the Ag mesoparticles can be tuned by changing the reduction speed. **Figure 3** shows the SEM and TEM images of Ag mesoparticles synthesized at a slow reduction speed (1% H_2O_2, 120 s). In the case of slow reduction, the Ag mesoparticles also retain the shape and size of Ag_2O templates, as shown in Figure 3a. However, the surfaces of the Ag mesoparticles obtained at the slow reduction speed become smooth and have numerous nanoholes, different from those obtained at quick reduction speed, as shown in Figure 3b. The TEM image in Figure 3c shows that the inner structure of Ag mesoparticles transforms from hollow mesocage to porous structure. The magnified TEM image in Figure 3d shows that the interior of mesoparticles is very porous. The SAED patterns (inset in Figure 3d) of the porous mesoparticles also reveal a polycrystalline nature similar to the Ag mesocage. The difference is due to the fact that the porous particles are composed of more and smaller nanocrystals.

The single-crystal Ag_2O particles (Figure S1, Supporting Information) were also used as sacrificial templates to synthesize Ag mesoparticles. SEM images of the obtained Ag mesoparticles are shown in **Figure 4**. Only Ag mesocages are obtained both at fast (10% H_2O_2) and slow (1% H_2O_2) reduction speeds. Moreover, their surface topography and inner structure are very similar, indicating that a relatively monotonous structure and surface topography can be obtained using single-crystal Ag_2O particles as sacrificial templates. More importantly, the surface is smoother than the highly rough Ag mesocage synthesized using the mesocrystal Ag_2O particles as sacrificial templates through quick reduction.

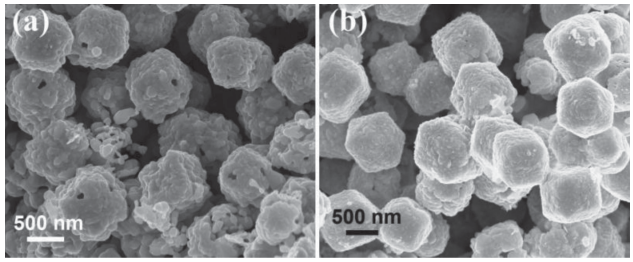

Figure 4. SEM images of Ag mesocages synthesized using single-crystal Ag_2O cubes as sacrificial templates under a) fast reduction (10% H_2O_2) and b) slow reduction (1% H_2O_2).

2.2. Growth Mechanism of Silver Mesoparticles

The intrinsic crystal structures of the Ag_2O particle templates significantly affect the final morphology and structure of Ag mesoparticles. On the basis of the experimental results, the following growth mechanism is proposed (**Figure 5**). For Ag mesoparticles synthesized using single-crystal Ag_2O particles (Figure 5a), the surface of Ag_2O particles is firstly reduced to form some non-uniform Ag nanoparticles (stage 1 in Figure 5a; experimental result in Figure S2, Supporting Information). With the ongoing reduction process, more Ag nanoparticles are produced and aggregate together to form a shell on the surface of Ag_2O particles (stage 2 and 3 in Figure 5a). In this process, the newly produced Ag atoms weld with the previously produced Ag nanoparticles, as illustrated in schemes A to D. Finally, a rough surface with numerous dents (indicated by arrows in scheme D) is formed on the Ag mesocage (Figure 5b).

Ag mesoparticles synthesized using mesocrystal Ag_2O particles as sacrificial templates show a different growth process, as illustrated in Figure 5c. Mesocrystal Ag_2O particles have a novel crystal structure, i.e., an ordered mesoscale superstructure composed of individual nanocrystals. In the reduction process, the building unit in the mesocrystal particle is separately reduced. Upon quick reduction, every building unit in the mesoparticle is reduced to form uniform individual spherical Ag nanoparticles that finally array on the mesocage surface to form a highly rough shell, as illustrated in schemes E to H. Thus, abundant deep and narrow nanogaps (indicated by arrows in scheme H) are formed between Ag nanoparticles on the surface of Ag mesocages (Figure 5d). For the SERS enhancement view, this kind of topography can potentially be an ideal single-particle SERS substrate with high enhancement. However, on the surface of conventional Ag mesocages obtained from single-crystal Ag_2O particles, only some shallow and irregular dents appear on the surface (Figure 5b). Under slow reduction, every building unit nanocrystal of mesocrystal Ag_2O particles is separately reduced to form small Ag hollow or porous nanoparticles. In this case, every unit corresponds to each small single-crystal Ag_2O particle being reduced. At the final stage, the produced individual small Ag hollow and porous particles connect with one another to form porous mesoparticles as shown in Figure 3.

2.3. SERS Properties of Silver Mesoparticles

The single-particle SERS activity of Ag mesoparticles synthesized using mesocrystal and single-crystal Ag_2O particles

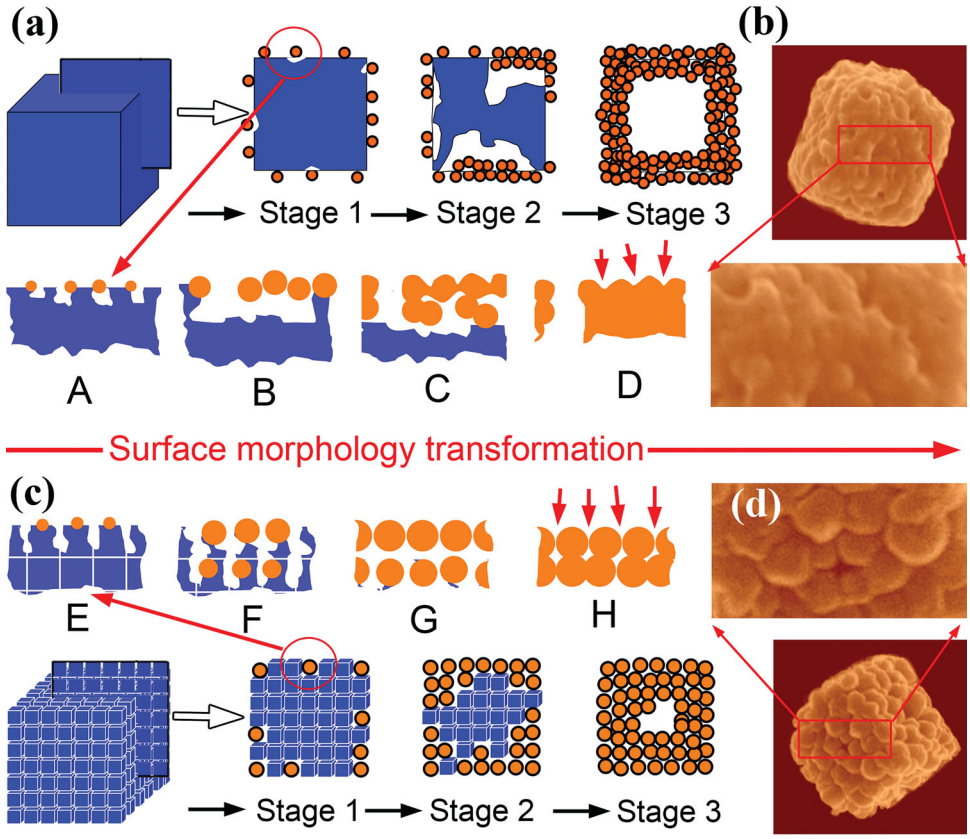

Figure 5. Schematic of the formation of Ag mesocages through the reduction of a) single-crystal and c) mesocrystal cubic Ag_2O particles. b,d) Different surface topographies showing the two kinds of particles.

as sacrificial templates were investigated under a confocal Raman microscope with laser excitation at 633 nm. A 11.0×10^{-9} M crystal violet (CV) aqueous solution, which is a standard SERS analyte,[39,40] was used by drop coating on the Si substrate sparsely coated with Ag mesoparticles. The individual Ag mesoparticle on the substrate can then be easily observed with an optical microscope. **Figure 6**a–c show the single-particle SERS spectra of individual Ag mesoparticles. The cubic highly rough-Ag mesocage synthesized using mesocrystal Ag_2O particles at quick reduction shows the highest single-particle SERS signal, which is approximately four times higher than individual Ag mesocages synthesized using single-crystal Ag_2O particles and roughly eight times higher than individual porous Ag cubic mesoparticles. Our previous study has shown that the average enhancement factor of single-particle Ag mesocage synthesized using single-crystal Ag_2O particle is found to be $\approx 10^8$ to 10^9.[23] In this study, the enhancement factor of single-particle highly rough Ag mesocage synthesized using mesocrystal Ag_2O particle is $\approx 10^9$. The enhancement factor was estimated using the same method as our previous work reported.[15,21,23,33] As shown in Figure 6d–f, SERS signal distributions across six separated highly rough-Ag mesocages were characterized (mapped) at a high spatial resolution of ≈200 nm provided by a high-magnification objective lens (100×) and confocal mode of the microscope (Method section). The "hot spots" over the six Ag mesocages are uniformly distributed throughout the entire surface of every Ag mesocage. Moreover, the intensities from each mesocage are uniform. This result clearly shows that the highly rough Ag mesocages possess very high SERS reproducibility that can be attributed to their uniform and highly rough surface topography.

To corroborate the observed relationship among SERS activity, structure and surface topography of various silver mesoparticles, 3D finite-difference time-domain (FDTD) simulation was used to calculate the local electric field intensity around model Ag particles irradiated with monochromatic light at 632 nm. The following four cubic model Ag particles (Supporting Information), which have the same external side length of 800 nm but different surface morphologies and inner structures, were studied: i) model A, a cubic mesocage with a shell constructed by a two-layer random arrangement of 100 nm nanoparticles and a 400 nm cubic hollow in the center (Figure S3, Supporting Information); ii) model B, a cubic mesocage with a shell randomly constructed by four layers and compactly aggregated 50 nm nanoparticles and a 400 nm cubic hollow in the center (Figure S4, Supporting Information); iii) model C, a filleted corner porous mesocube with ellipse holes on the surface (Figure S5, Supporting Information); and iv) model D, a core–shell cubic mesoparticle with a same shell constructed with model A, but the center is solid. In this study, models A to C were used to simulate these three kinds of mesoparticles studied for SERS properties (insets in Figure 6a–c), respectively.

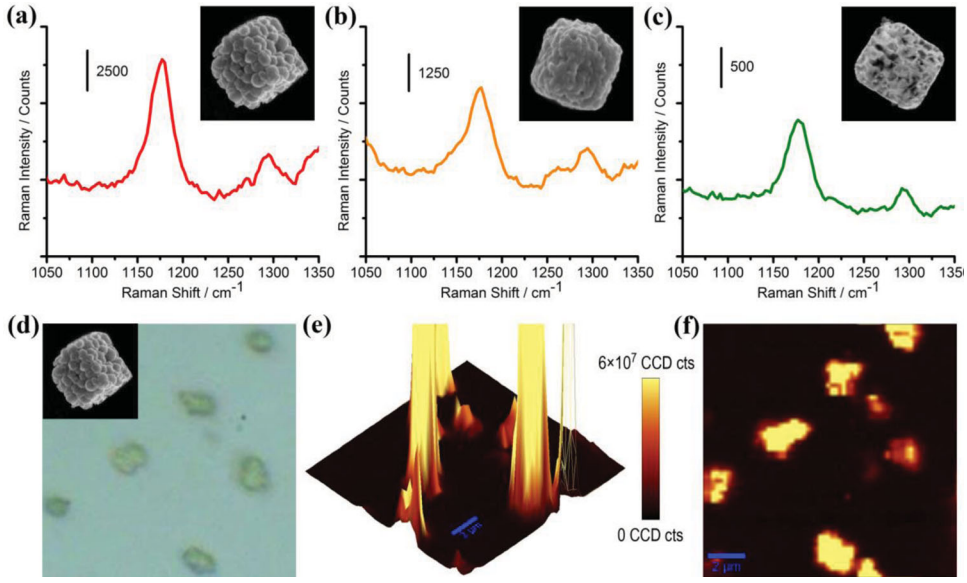

Figure 6. Single-particle SERS spectra of CV molecules on a) highly rough Ag mesocage, b) conventional Ag mesocage, and c) porous Ag particles. d) Optical microscopy image of a substrate with individual highly rough Ag mesocages synthesized using mesocrystal Ag_2O particles under quick reduction as well as correlated e) two- and c) three-dimensional Raman images. The color-coded signal in the Raman images corresponds to the intensity of the Raman band of CV at 1172 cm^{-1} integrated over 1120–1250 cm^{-1} after background subtraction.

The Raman intensity is generally accepted to increase by a factor $|E|^4$ with respect to the local electric field on the SERS substrate surface.[41] **Figure 7**a–c show the typical distributions of the electric field strength E (plotted as color-coded $|E|^2$) obtained from models A to C. Similar to the experimental result, the most localized and enhanced electric field regions are found throughout the entire surface of model A. The maximal $|E|^2$ enhancement is found to be approximately 2800, 1200, and 300 for models A, B, and C, respectively. Regarding the factor $|E|^4$, the value of model A is approximately five times higher

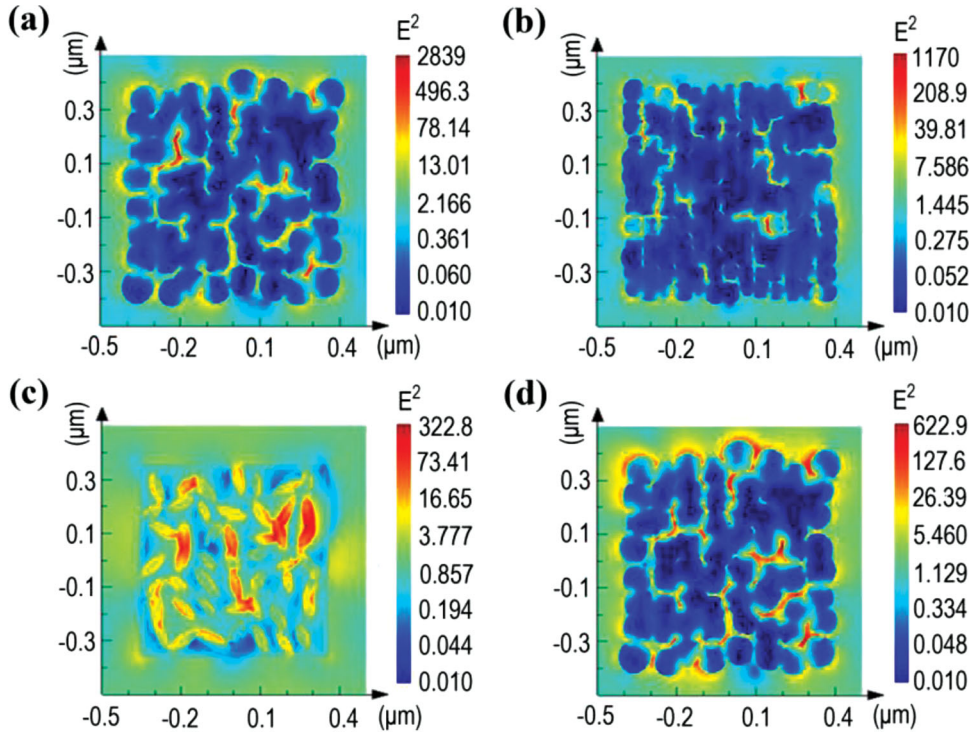

Figure 7. Corresponding calculated distributions of the local electric field intensity (color-coded relative E^2 values) across air-suspended model Ag cubic mesoparticles irradiated from the top with a 632 nm laser. a) Ag cubic mesocage with a highly rough surface, b) Ag cubic mesocage with a lowly rough surface, c) porous Ag cubic mesoparticle, and d) solid Ag cubic mesoparticle with a highly rough surface.

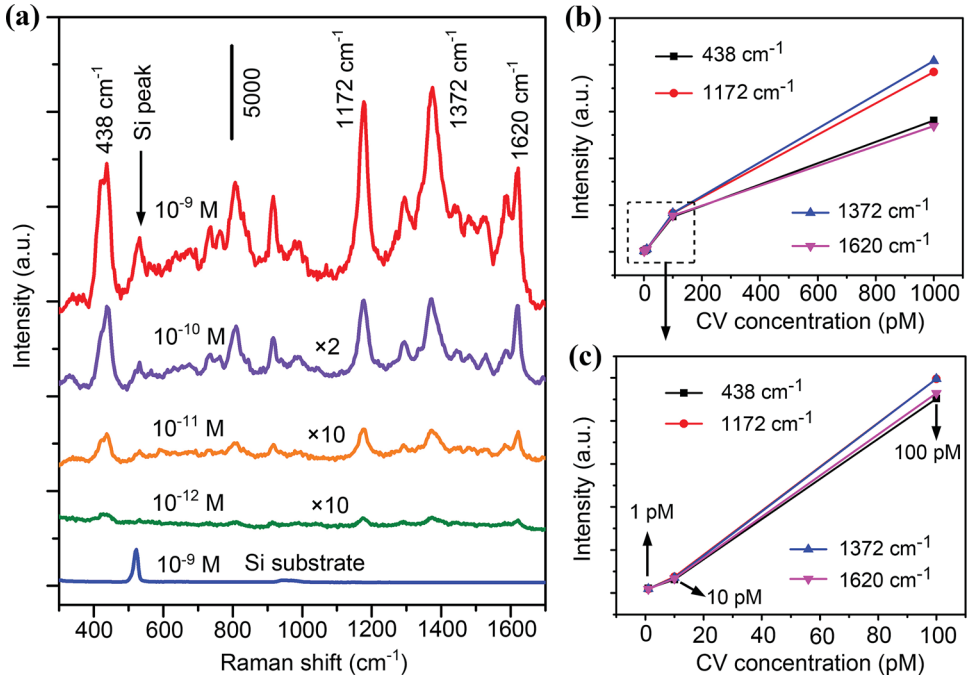

Figure 8. a) Single-particle SERS spectra of CV molecules adsorbed on an Ag mesocage synthesized using mesocrystal Ag_2O particles under quick reduction at decreased CV concentrations from 10^{-9} M to 10^{-12} M. b) SERS intensity plot at four fingerprint peaks (438, 1172, 1372, and 1620 cm^{-1}) as a function of the CV concentration. c) The magnified plot of circled area in (b).

than that of model B, which well agrees with the experiment result (approximately four times, Figure 6a,b).

On the basis of the intensity maps of the local electric field in Figure 7a, the "hot spot" is found to be distributed in the crevices and junctions between the arrayed nanoparticle units on the mesocage shell because of strong plasmon coupling between nanoparticles. Generally, the local electric field is enhanced by two kinds of rough topographic structures. One is the vicinity of sharp tips with high curvatures that acts as nano-antenna enhancement, and the other is the slit area between two metal nanoparticles that serve as nanogap enhancement. The Raman scattering of a molecule can be greatly enhanced when the molecule is situated on or near the regions of nano-texted curvatures or gaps on rough metal surfaces.[42–45] In these regions, the collective oscillation of conduction electrons is confined and results in so-called localized surface plasmon resonance under the light irradiation within a certain wavelength range.[46–49] The plasmonic coupling effect in these regions induces very high local electromagnetic fields that generate "hot spots" with high SERS enhancement (enhancement factor up to 10^{10}–10^{11}), even for single-molecule detection.[5,19,50,51] In this study, the enhanced local electric field in models A to C is mainly excited by a nanohole or nanoslit on the Ag mesoparticle surface that serves as nanogap enhancement. Compared with models B and C, the deeper and narrower slit on the particle surface of model A can more effectively confine light in the slit cavity, thereby resulting in a stronger localized electric field excited at its narrow slit area by the confined light. Compared with model D (Figure 7d), the hollow structure of model A can help the light to interact further with the particles on the mesocage shell, resulting in stronger surface plasmonic field from the coupling between surface plasmon fields on exterior and interior shells.[4] The FDTD simulation result indicates that the great deal of deep and narrow slits constructed by array of nanoparticle units on the highly rough-Ag mesocages synthesized using the mesocrystal Ag_2O particles and their hollow structure can greatly improve SERS enhancement.

The extreme limit of single–particle SERS versus analyte concentration was evaluated on highly rough-Ag mesocages synthesized using mesocrystal Ag_2O particles, as shown in **Figure 8**. In this study, quite diluted solution of CV in water with concentrations from 1.0×10^{-9} to 1.0×10^{-12} M was used by depositing in the mesocages substrate as described in the Experimental Section. The average numbers of CV molecules on single Ag mesocage at concentrations of 1.0×10^{-12}, 1.0×10^{-11}, 1.0×10^{-10}, and 1.0×10^{-9} M were estimated as 3.8, 38, 380, and 3800, respectively (Supporting Information). Figure 8a shows that when the CV concentration decreases to 1.0×10^{-12} M, the spectral features close to the characteristic vibrational peaks of CV (438, 1172, 1372, and 1620 cm^{-1}) can still be easily identified on an individual Ag mesocage and well corresponds to the ordinary Raman spectra of CV in the solid state and in the aqueous solution. This unprecedently low detection limit corresponds to about 3.8 CV molecules on the detected individual single Ag mesocages, indicating only a few molecular-level detection. Our previous study showed that the concentration extreme limit for the Ag mesocage synthesized using the single-crystal Ag_2O particle as a sacrificial template was 1.0×10^{-11} M (corresponding to 38 CV molecules on the single Ag particle).[23] In Ko et al.,[52] the detection limit on porous substrate corresponds to 30 DNT

molecules. So, the detection limit is greatly improved on the highly rough Ag mesocage synthesized using mesocrystal Ag_2O particle as a sacrificial template.

Usually, only the CV molecules adsorbed at "hot spots" contribute to the Raman signal intensity. As such, SERS measurements with silver nanospheres substrate showed that, of 1 000 000 SERS active sites, 63 sites contributed 24% of the overall SERS intensity. On the individual highly rough Ag mesocage, the detection limit decreases to several molecules level, indicating that the probability of CV molecules adsorbing at "hot spots" is very high. As shown in previous FDTD simulation, on the surface of Ag mesocage, the "hot spots" located at the nanogaps between Ag nanoparticle units. Molecular dynamic simulation result shows that the CV molecule preferably adsorbs at or near to these "hot spots" (nanogaps) on the Ag mesocage surface (Supporting Information). The molecular dynamic simulation is similar with previous report,[21,53] and details are described in the Supporting Information. The prior adsorption of CV molecules at "hot spots" can well explain why the detection limit can be decreased to several molecules for the single-particle SERS.

The signal intensity changes of single-particle SERS for CV concentrations of 1.0×10^{-12}–1.0×10^{-9} M are shown in Figure 8b. The Raman intensity increases with the increase of CV concentration. At low concentration scopes, the increase of Raman intensity keeps an almost linear relationship with concentration as shown in Figure 8c, indicating that the most of added new CV molecules on the mesocage same as the previous adsorbed molecules have contribution to the Raman intensity with the increase of concentration. The linear relationship keeps with concentration increasing from 1 to 100×10^{-12} M (number of CV molecules increasing from ≈3.8 to ≈380 on single Ag mesocage). When the most of "hot spots" on the Ag mesocage have been occupied by adsorbed CV molecules, the probability of new added CV molecules adsorbing at "hot spots" becomes lower, resulting in the Raman intensity increase can not continuously keep linear relationship with the concentration increasing to higher level (Figure 8b, 1000×10^{-12} M).

3. Conclusion

Mesocrystal particles are used for the first time as a sacrificial template to prepare Ag mesoparticles. In the reduction process, each nanocrystal unit in mesocrystal Ag_2O particles, which corresponds to a small single-crystal Ag_2O particle, is separately reduced into uniform Ag nanoparticles at quick reduction speed or hollow nanocage at slow reduction speed. These Ag nanoparticles self-assemble to form highly rough Ag hollow mesocages or porous mesoparticles with controllable surface topography. Compared with porous Ag mesoparticle and conventional Ag mesocage synthesized using single-crystal AgO particles, highly rough Ag mesocage shows an unusual higher single-particle SERS enhancement (about 10^9). Abundant deep and narrow nanogaps on the shell of the highly rough Ag mesocage induces a strong localized electric field that can be excited by monochromatic light, thereby exerting multiple effective "hot spots" homogeneously distributed on the surface. The extreme limit of single-particle SERS versus analyte concentration is sensitive even at concentrations as low as 1.0×10^{-12} M, corresponding to several molecules detection. Thus, a new type of highly rough Ag mesoparticles is obtained by an easy particle-mediated protocol. The mesoparticles have high single-particle SERS sensitivity, caused by the highly rough surface, anisotropic shape effect, and "less-lossy" compared with gold within the blue/green visible range.[54]

4. Experimental Section

Synthesis of Ag_2O Particles: All chemicals were used as received without further purification. Single-crystal Ag_2O particles were synthesized by a facile solution-phase route referring to our previous report.[23] In the synthesis, 0.5 M ammonia was added in a dropwise manner into 50 mL 1×10^{-3} M $AgNO_3$ aqueous solution in the presence of 0.1×10^{-3} M poly (vinyl pyrrolidone) (PVP, Mw = 55 000 amu) until the color of the solution turned from tawny to colorless and transparent solution. Following, 0.3 mL of 2 M NaOH was rapidly injected into the above solution by stirring. Immediately, brownish-black precipitates were obtained, which were collected by centrifugation and washed several times with double-distilled water as well as absolute ethanol. Mesocrystal Ag_2O particles were synthesized using an electrochemistry method referring to our previous report.[36] In a double-electrode electrodeposition system, two parallel silver plates with dimension 5 mm × 5 mm × 0.5 mm were separated by a distance of 3 cm in a 1×10^{-3} M $AgNO_3$ aqueous solution as anode and cathode. A direct current potential with 15 V was applied between the two silver plates electrodes. As electric current passed between the two electrodes, brown-colored deposits would emerge in the vicinity of the anode and fall off into the solutions, which were collected for further investigation and reaction.

Synthesis of Ag Particles: In a typical synthesis, the obtained Ag_2O particles were dispersed into 10-mL double-distilled water. Then, 20 mL of hydrogen peroxide (10%) was added into the solution by dropwise while magnetic stirring. The solution immediately changed color and evolved gas. After 120 s, the precipitates in the solution were isolated by centrifugation (2 000 rpm, 10 min) and then washed several times with water and finally dispersed in ethanol for further characterization.

Characterization: The morphology of the products was investigated by field emission SEM using a JEOL (JSM-7000F) at an accelerating voltage of 20 kV. TEM analysis images and SAED pattern analysis were performed on a JEOL JEM-2100 transmission electron microscope operating at an accelerating voltage of 200 kV.

SERS Measurement: To evaluate SERS performance, 0.1 mL of the 1.0×10^{-9} M aqueous CV solution was dropped onto the wafer piece (with an area of 10 mm × 10 mm) coated by synthesized silver mesocages, rinsed with deionized water, and dried under ambient conditions. SERS measurements were carried in backscattering geometry using a WiTec CRM200 confocal Raman microscope and a Kaiser Optical RXN1 spectrometer with the 633 nm He–Ne laser line at room temperature. The excitation laser spot size and intensity on the samples were typically ≈3 μm in diameter (i.e., significantly larger than a single mesoparticle size) and 0.1 mW after being decreased with a D2 attenuation piece, respectively. Raman imaging of "hot spots" was performed on the CRM200 microscope employing a piezo table for sample scanning with a typical X–Y step of 200 nm (200 nm × 200 nm scanning pixel size), a high-resolution 100× objective (≈0.5 μm laser spot) and a spectrum acquisition time of 2 s per pixel. Raman images represent a color-coded area of the characteristic Raman band of CV at 1172 cm^{-1} integrated over 1120–1250 cm^{-1} with a subtracted broad background signal.

FDTD Simulation: Four models based on the SERS samples were built and their geometric details are shown in the Supporting Information. The 3D FDTD simulation was used to calculate the near-field electric field intensity at excitation wavelengths of 632 nm. The incident light was a plane wave propagating along the z-axis and polarized along the x-axis. It was assumed that each geometrical model was suspended in air (n_0 = 1.0). The frequency (ω) dispersive and complex dielectric

function for Ag, ε_{Ag} (ω), were obtained from the handbook of optical materials. The grid size was 5 nm and the size of the cross section of electric field intensity was $1.0 \times 1.0\ \mu m^2$.

Supporting Information

Supporting Information is available from the Wiley Online Library or from the author.

Acknowledgements

This work was supported by National Natural Science Foundation of China (grant nos. 51171139 and 51201122), Natural Science Foundation of Shaanxi Province (grant no. 2012JQ6006), Doctoral Fund for New Teachers (nos. 20120201120049 and 20110201120039), Tengfei Talent Project of Xi'an Jiaotong University, New Century Excellent Talents in University (NCET), Scientific New Star Program in Shann Xi Province (No.2012KJXX-03), and Fundamental Research Funds for the Central Universities.

Received: August 21, 2013
Published online: September 17, 2013

[1] Y. G. Sun, B. Mayers, Y. N. Xia, *Adv. Mater.* **2003**, *15*, 641.
[2] Q. Zhang, W. Wang, J. Goebl, Y. Yin, *Nano Today* **2009**, *4*, 494.
[3] S. E. Skrabalak, J. Chen, Y. Sun, X. Lu, L. Au, C. M. Cobley, Y. Xia, *Acc. Chem. Res.* **2008**, *41*, 1587.
[4] M. A. Mahmoud, M. A. El-Sayed, *J. Am. Chem. Soc.* **2010**, *132*, 12704.
[5] M. Rycenga, X. H. Xia, C. H. Moran, F. Zhou, D. Qin, Z. Y. Li, Y. A. Xia, *Angew. Chem. Int. Ed.* **2011**, *50*, 5473.
[6] J. F. Li, Y. F. Huang, Y. Ding, Z. L. Yang, S. B. Li, X. S. Zhou, F. R. Fan, W. Zhang, Z. Y. Zhou, D. Y. Wu, B. Ren, Z. L. Wang, Z. Q. Tian, *Nature* **2010**, *464*, 392.
[7] Y. Fang, N. H. Seong, D. D. Dlott, *Science* **2008**, *321*, 388.
[8] E. J. Smythe, M. D. Dickey, J. M. Bao, G. M. Whitesides, F. Capasso, *Nano Lett.* **2009**, *9*, 1132.
[9] S. M. Nie, S. R. Emery, *Science* **1997**, *275*, 1102.
[10] Z. Chen, S. M. Tabakman, A. P. Goodwin, M. G. Kattah, D. Daranciang, X. R. Wang, G. Y. Zhang, X. L. Li, Z. Liu, P. J. Utz, K. L. Jiang, S. S. Fan, H. J. Dai, *Nat. Biotechnol.* **2008**, *26*, 1285.
[11] J. N. Anker, W. P. Hall, O. Lyandres, N. C. Shah, J. Zhao, R. P. Van Duyne, *Nat. Mater.* **2008**, *7*, 442.
[12] Z.-Y. Li, Y. Xia, *Nano Lett.* **2010**, *10*, 243.
[13] H. Ko, S. Singamaneni, V. V. Tsukruk, *Small* **2008**, *4*, 1576.
[14] H. J. You, Y. T. Ji, L. Wang, S. C. Yang, Z. M. Yang, J. X. Fang, X. P. Song, B. J. Ding, *J. Mater. Chem.* **2012**, *22*, 1998.
[15] J. X. Fang, S. Y. Du, S. Lebedkin, Z. Y. Li, R. Kruk, M. Kappes, H. Hahn, *Nano Lett.* **2010**, *10*, 5006.
[16] J. M. Nam, D. K. Lim, K. S. Jeon, J. H. Hwang, H. Kim, S. Kwon, Y. D. Suh, *Nat. Nanotechnol.* **2011**, *6*, 452.
[17] D. Graham, D. G. Thompson, W. E. Smith, K. Faulds, *Nat. Nanotechnol.* **2008**, *3*, 548.
[18] C. F. Tian, Z. Liu, J. H. Jin, S. Lebedkin, C. Huang, H. J. You, R. Liu, L. Q. Wang, X. P. Song, B. J. Ding, M. Barczewski, T. Schimmel, J. X. Fang, *Nanotechnology* **2012**, *23*, 165604.
[19] M. J. Mulvihill, X. Y. Ling, J. Henzie, P. D. Yang, *J. Am. Chem. Soc.* **2010**, *132*, 268.
[20] H. Wang, N. J. Halas, *Adv. Mater.* **2008**, *20*, 820.
[21] Z. Liu, F. Zhang, Z. Yang, H. You, C. Tian, Z. Li, J. Fang, *J. Mater. Chem. C* **2013**, *1*, 5567.
[22] H. Y. Liang, Z. P. Li, W. Z. Wang, Y. S. Wu, H. X. Xu, *Adv. Mater.* **2009**, *21*, 4614.
[23] J. X. Fang, S. Y. Liu, Z. Y. Li, *Biomaterials* **2011**, *32*, 4877.
[24] L. Zhang, X. Lang, A. Hirata, M. Chen, *ACS Nano* **2011**, *5*, 4407.
[25] H. You, S. Yang, B. Ding, H. Yang, *Chem. Soc. Rev.* **2013**, *42*, 2880.
[26] Z. Peng, H. You, J. Wu, H. Yang, *Nano Lett.* **2010**, *10*, 1492.
[27] X. Lu, H.-Y. Tuan, J. Chen, Z.-Y. Li, B. A. Korgel, Y. Xia, *J. Am. Chem. Soc.* **2007**, *129*, 1733.
[28] Y. G. Sun, Y. N. Xia, *Science* **2002**, *298*, 2176.
[29] T. Li, H. You, M. Xu, X. Song, J. Fang, *ACS Appl. Mater. Inter.* **2012**, *4*, 6942.
[30] R. Pasricha, T. Bala, A. V. Biradar, S. Umbarkar, M. Sastry, *Small* **2009**, *5*, 1467.
[31] H. P. Liang, H. M. Zhang, J. S. Hu, Y. G. Guo, L. J. Wan, C. L. Bai, *Angew. Chem. Int. Ed.* **2004**, *43*, 1540.
[32] F. Hong, S. Sun, H. You, S. Yang, J. Fang, S. Guo, Z. Yang, B. Ding, X. Song, *Cryst. Growth Des.* **2011**, *11*, 3694.
[33] J. X. Fang, S. Lebedkin, S. C. Yang, H. Hahn, *Chem. Commun.* **2011**, *47*, 5157.
[34] H. Colfen, M. Antonietti, *Angew. Chem. Int. Ed.* **2005**, *44*, 5576.
[35] J. Fang, B. Ding, H. Gleiter, *Chem. Soc. Rev.* **2011**, *40*, 5347.
[36] J. X. Fang, P. M. Leufke, R. Kruk, D. Wang, T. Scherer, H. Hahn, *Nano Today* **2010**, *5*, 175.
[37] F. G. Xu, K. Cui, Y. J. Sun, C. L. Guo, Z. L. Liu, Y. Zhang, Y. Shi, Z. A. Li, *Talanta* **2010**, *82*, 1845.
[38] J. X. Fang, H. J. You, P. Kong, Y. Yi, X. P. Song, B. J. Ding, *Cryst. Growth Des.* **2007**, *7*, 864.
[39] X. M. Qian, S. M. Nie, *Chem. Soc. Rev.* **2008**, *37*, 912.
[40] K. Kneipp, Y. Wang, H. Kneipp, L. T. Perelman, I. Itzkan, R. Dasari, M. S. Feld, *Phys. Rev. Lett.* **1997**, *78*, 1667.
[41] P. Dawson, J. A. Duenas, M. G. Boyle, M. D. Doherty, S. E. J. Bell, A. M. Kern, O. J. F. Martin, A. S. Teh, K. B. K. Teo, W. I. Milne, *Nano Lett.* **2011**, *11*, 365.
[42] M. G. Albrecht, J. A. Creighton, *J. Am. Chem. Soc.* **1977**, *99*, 5215.
[43] D. L. Jeanmaire, R. P. Vanduyne, *J. Electroanal. Chem.* **1977**, *84*, 1.
[44] M. Moskovits, *Rev. Mod. Phys.* **1985**, *57*, 783.
[45] S. K. Ghosh, T. Pal, *Chem. Rev.* **2007**, *107*, 4797.
[46] K. A. Stoerzinger, J. Y. Lin, T. W. Odom, *Chem. Sci.* **2011**, *2*, 1435.
[47] L. M. Tong, T. Zhu, Z. F. Liu, *Chem. Soc. Rev.* **2011**, *40*, 1296.
[48] C. F. Tian, C. H. Ding, S. Y. Liu, S. C. Yang, X. P. Song, B. J. Ding, Z. Y. Li, J. X. Fang, *ACS Nano* **2011**, *5*, 9442.
[49] H. Wang, D. W. Brandl, P. Nordlander, N. J. Halas, *Acc. Chem. Res.* **2007**, *40*, 53.
[50] H. X. Xu, E. J. Bjerneld, M. Kall, L. Borjesson, *Phys. Rev. Lett.* **1999**, *83*, 4357.
[51] A. M. Michaels, J. Jiang, L. Brus, *J. Phys. Chem. B* **2000**, *104*, 11965.
[52] H. Ko, S. Chang, V. V. Tsukruk, *ACS Nano* **2008**, *3*, 181.
[53] Z. M. Peng, H. J. You, H. Yang, *ACS Nano* **2010**, *4*, 1501.
[54] P. G. Etchegoin, E. C. Le Ru, *Phys. Chem. Chem. Phys.* **2008**, *10*, 6079.